The Pennsylvania State University

The Graduate School

Department of Aerospace Engineering

DELTA-V FEASIBILITY OF PIGGYBACK LUNAR TRANSFERS

A Thesis in

Aerospace Engineering

by

Skyler Shuford

Submitted in Partial Fulfillment
of the Requirements
for the Degree of

Master of Science

December 2015

The thesis of Skyler Shuford was reviewed and approved* by the following:

David B. Spencer
Professor of Aerospace Engineering
Thesis Advisor

Robert G. Melton
Professor of Aerospace Engineering and Director of Undergraduate Studies

George A. Lesieutre
Professor of Aerospace Engineering
Head of the Department of Aerospace Engineering

*Signatures are on file in the Graduate School

ABSTRACT

This thesis presents the results of analysis to determine the feasibility of lunar missions as secondary, piggyback payloads. Piggyback missions are becoming increasingly common as lower cost options to space. It is shown that piggyback, flyby (or crash) lunar missions are feasible departing from the International Space Station (ISS) orbit, geosynchronous orbit (GEO), geotransfer orbit (GTO), and sun-synchronous orbit. Trajectories from GEO are feasible any time throughout the lunar period, with varying departure windows above 150° longitude. Trajectories from GTO have the lowest transfer ΔV with a minimum of 0.7 km/s and also large departure windows up to 200° longitude. Trajectories from GEO and GTO have similar required capture ΔV of about 2 km/s, although more analysis is necessary for optimality. Capture trajectories from ISS and sun-synchronous orbit may not be feasible with existing propulsion capabilities.

TABLE OF CONTENTS

LIST OF FIGURES

LIST OF TABLES

ACKNOWLEDGEMENTS

I would like to begin by thanking my advisor, Dr. Spencer, for his support and flexibility throughout my time attaining my Master of Science degree. From the beginning, Dr. Spencer acted as a mentor, not just in academia, but in my career. Because of Dr. Spencer, I was able to secure opportunities within Penn State and the aerospace industry. Additionally, I had been a little over-ambitious with my timeline considering I accepted a more-than-full-time internship while I wrote this thesis. He was very understanding of my life outside of academia, and therefore I could accept an internship that helped serve as catalyst for a fantastic full-time position. I am grateful that I was able to take this internship even though it pushed back completion of my degree. My over-ambition also led me to book an extended vacation, which ended up falling prior to completion of this thesis. The vacation, while a nice mental break, was not a necessity, so Dr. Spencer's acceptance of these travels was great. I also really appreciate the quick responses and suggestions while I worked remotely. I owe Dr. Spencer a lot, and am thankful for all his help.

My second thanks goes to my parents, Mike and Debbie Shuford. In addition to the whole birth thing, they have supported me in every way: financially, emotionally, in my career. All my successes would not have been possible without their love and guidance. I hope that my successes continue, so I can make a small dent in repaying them in some way.

Finally, I would like to thank my girlfriend, Colette Long, for her cross-country encouragement while I was working on this degree. Moving to a new state where I knew no one, while a growing experience, was difficult, but being able to call her gave me the foundation to expand in this new place.

Chapter 1

Introduction

It is becoming increasingly necessary to understand the propulsive cost (ΔV) tradespace for lunar transfers as more and more organizations plan missions to the moon. The moon still offers an abundance of science opportunities, which is more desirable as the cost to reach the moon decreases. Payload sharing is becoming much more common to reduce the launch vehicle costs per shared payload volume. However, this can limit or completely define the spacecraft orbit after release from the launch vehicle, especially when spacecraft is secondary payload. Consequently, it is useful to analyze the ΔV costs of reaching the moon from suboptimal initial orbits.

Geosynchronous, geotransfer, low-Earth orbits are commonly used orbits by primary payloads, thus, there is a high likelihood of a secondary payload option for these orbits. In general, these orbits are suboptimal for lunar transfer. However, a suboptimal solution may be feasible depending on the mission specific propellant budget of the secondary payload.

Problem Statement

This thesis presents the analysis for lunar transfers from initial orbits that are either geosynchronous orbits, geosynchronous transfer orbits, low-Earth orbits that match the International Space Station (ISS) orbit and sun-synchronous orbits. It could serve as a guide for initial mission designs for lunar missions flying as secondary payloads.

This thesis begins with background material (Chapter 2) that is necessary to understand the problem and results. It begins with explanation of the present state of the secondary payload

industry, especially in relation to lunar science. It covers four of the common orbits and explains the various parameters that define these orbits. It then explains two common theories in orbital mechanics that are relevant to lunar transfers: Hohmann transfers and Lambert's problem.

Explanation of the included analysis is found in Chapter 3. This chapter begins by explaining the numerical method used to analyze the lunar transfers. This includes the propagation method, forces acting on the simulated spacecraft, and explanation of the effects of this problem type on the numerical method (ie: stiffness). The equations of Lambert's problem are introduced, which were solved using an open-source solver. A method for estimating capture ΔV is introduced for the purpose of providing a full description, although comprehensive capture analysis is outside the scope of this thesis. The analysis chapter is concluded with a step-by-step explanation of the simulation setup and execution.

Chapter 4 presents the results of the analysis and discusses the consequences of the four departure orbits. The primary feasibility metric is ΔV. For each initial orbit, the chapter explains how the ΔV relates to departure and transit conditions. Orbit visualizations are presented for geometric understanding. The chapter concludes with a brief discussion of lunar capture.

Chapter 5 concludes this thesis. It consists of a summary of the trajectory analysis and relates the results to the real-life application feasibility. This chapter wraps up with suggestions for future work.

Chapter 2

Background

This analysis focuses on studying the options for lunar missions based on highest number of opportunities. Launch vehicles such as United Launch Alliance's Atlas V and Delta IV and the SpaceX Falcon 9 are able to put spacecraft on translunar trajectories as primary payloads, but this is expensive and limits the number of opportunities to reach the moon [1][2]. Flying piggyback missions as secondary payload gives the spacecraft developer more power and opportunity to reach the due to increased launch opportunities and lower costs.

Secondary Payloads

There are a few standards used to design and fly spacecraft as secondary payloads. The most common is the cubesat standard. A 1-unit (1U) cubesat fits in a 10 centimeter cube and has a mass less than 1.33 kilograms [3]. There are also 3U and 6U (two by three) variants, which are commonly flown. Companies such as Aerojet are designing propulsion systems that will fit into the standard cubesat envelope [4], allowing ΔV maneuvers for the previously passive spacecraft. Another standard spacecraft is the ESPA class (see Fig. 2.1), which allows for a 61 cm x 71 cm x 97 cm satellite with less than 180 kg mass [5]. This provides more mass and volume for larger propulsion systems.

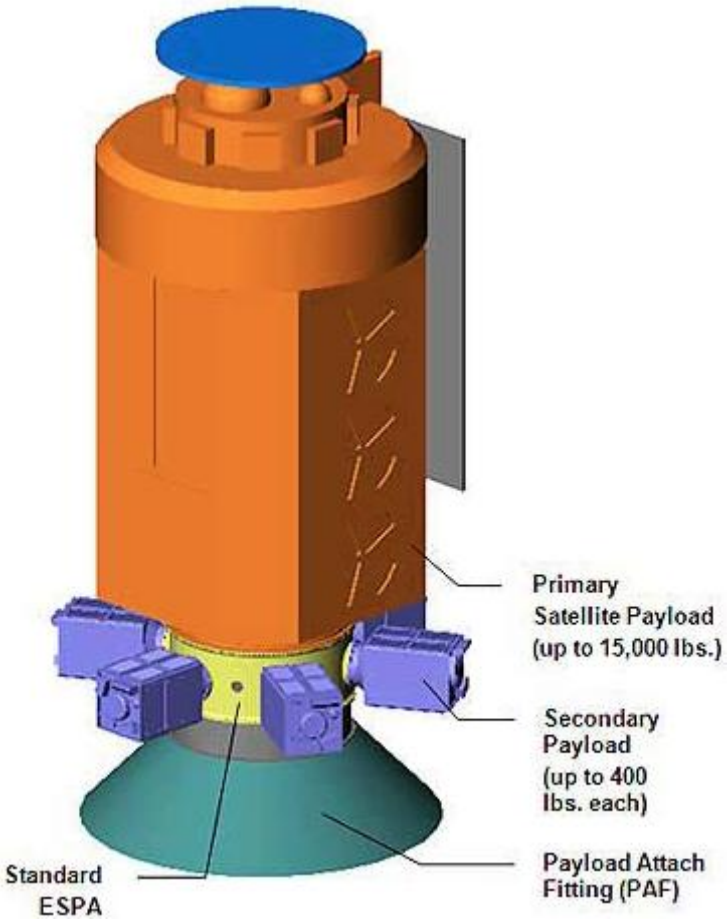

Figure 2.1: Model showing integrated ESPA secondary payloads. Courtesy Milsat Magazine[1].

In addition to other secondary payload standards, non-standard payload sharing may become commonplace. In payload sharing, fairing volume is subdivided and allocated to multiple spacecraft, in order to share the costs of the rocket launch.

Orbital Definitions

There are many parameters used to define and analyze orbits. These parameters are generally geometric, and allow analysts to use intuition and visualization more easily.

[1] http://www.milsatmagazine.com/story.php?number=797849281 [retrieved 27 November 2015]

Earth-Centered Inertial

The Earth-Centered Inertial (ECI) coordinate frame is defined by the Z-axis through the North pole, and the X-axis in the equatorial plane pointing to vernal equinox, with the Y-axis completing the right-handed coordinate frame. Vernal equinox is defined by the vector from the Earth to the Sun when coplanar with the equator. Figure 2.3 shows the inertial axes. The ECI coordinate frame is used for this analysis.

Orbital Elements

Kepler defined six parameters that fully define an orbit in a two-body system with one infinitesimal mass [6]. These are eccentricity (oblateness of the orbit), semimajor axis (a), inclination (i), right ascension of the ascending node (RAAN, Ω), argument of periapse (ω), and mean anomaly. Alternatively, true anomaly (θ) can be substituted for mean anomaly, and has been in this thesis. Figure 2.2 shows the orbital shape where F is the focus (and location of the central body), and F^* is the empty focus. Figure 2.3 illustrates the orbital elements (excluding semimajor axis and eccentricity). Equation 2.1 shows the equation for eccentricity, which is defined by radius of apoapse (r_a) and radius of periapse (r_p).

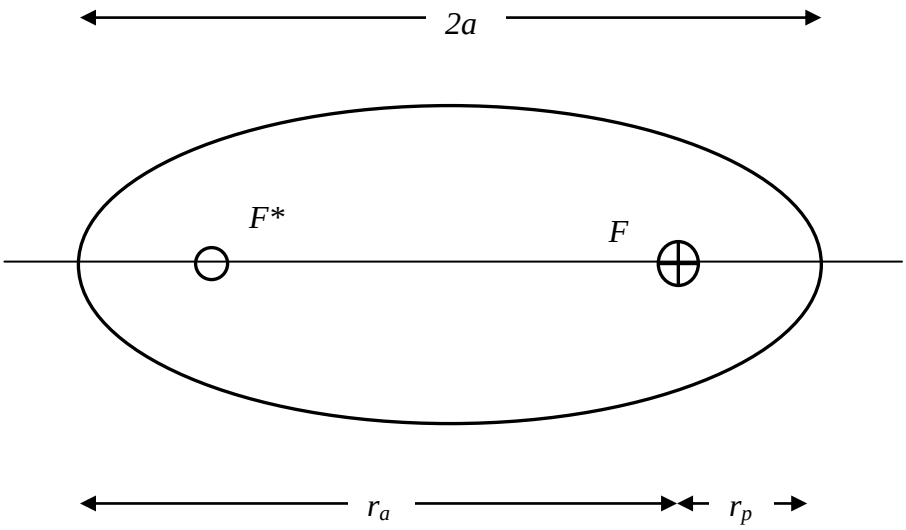

Figure 2.2: Orbital shape definitions

$$e = \frac{r_a - r_p}{r_a + r_p} \tag{2.1}$$

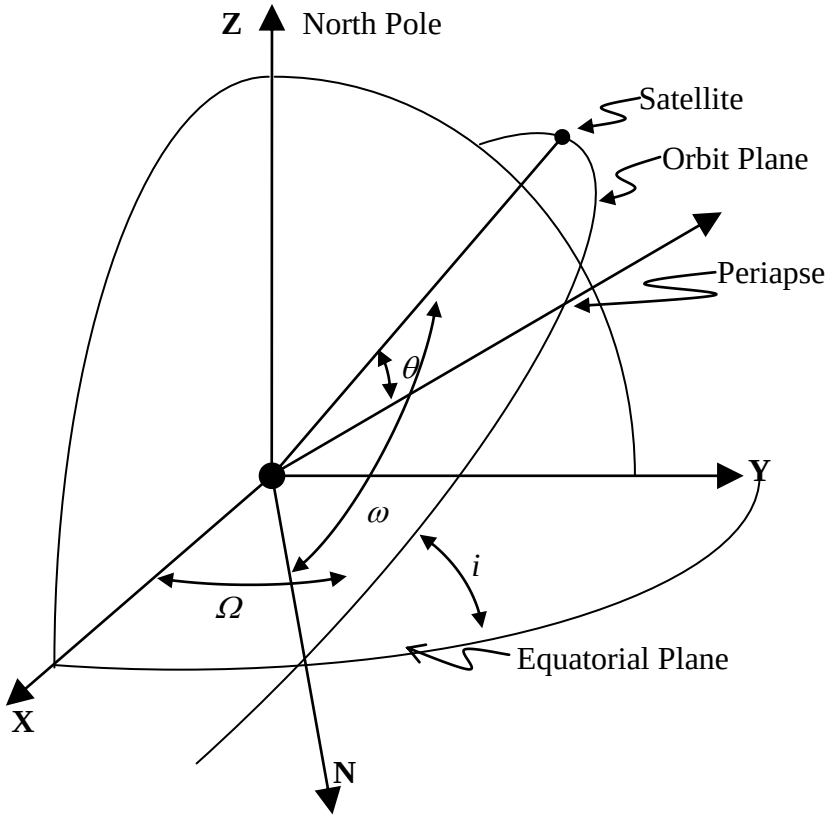

Figure 2.3: Definitions of orbital elements

Semimajor Axis and Orbital Period

Semimajor axis defines half of the distance from periapse (lowest altitude point in orbit) to apoapse (highest altitude point in orbit). Additionally, semimajor axis, *a*, defines the orbital period

$$T = 2\pi\sqrt{\frac{a^3}{\mu}} \tag{2.2}$$

where T is the orbital period, and μ is the gravitational parameter of the central body.

Common Orbits

This analysis covers four orbits that are the final destination for many primary payloads. These four orbits are the destination for launches multiple times per year. As a secondary payload, this is ideal since it increases the number of potential launch opportunities. Table 2.1 shows estimated values for the four orbits discussed in this thesis.

Table 2.1: Orbit type and parameter table

Orbit Type	Semimajor Axis	Eccentricity	Inclination	RAAN	Argument of Periapse	True Anomaly
LEO	6578 km to 7278 km	0 to 0.1	0° to 100°	0° to 360°	0° to 360°	0° to 360°
Sun-synchronous	6578 km to 7278 km	0 to 0.1	90° to 100°	0° to 360°	0° to 360°	0° to 360°
GTO	23000 km to 35000 km	> 0.5	0°	0° to 360°	0° to 360°	0° to 360°
GEO	42164 km	0	0°	0° to 360°	0° to 360°	0° to 360°

Low-Earth Orbit

Low-Earth Orbit (LEO) is defined by an altitude below 3000 km, with most below 900 km [1]. Spacecraft in LEO generally fly in near circular orbits. Of the subsequent orbits, LEO requires the lowest energy to reach, but spacecraft in these orbits have the highest orbital speeds, which are generally around 7.5 km/s. Example spacecraft that fly in LEO include surveillance satellites, remote sensing science satellites, and the International Space Station.

International Space Station Orbit

The International Space Station receives frequent visits to bring supplies and astronauts and to remove waste and bring astronauts back to Earth. The ISS's nominal orbital altitude is around 250 miles and has an inclination of 51.6° [7]. Due to a small amount drag caused by the low-density upper atmosphere, this orbit slowly decays and the ISS is boosted to maintain the orbit.

Sun-synchronous Orbit

Sun-synchronous orbits are low-Earth orbits with inclinations near 98°, called such because they maintain orientation with respect to the sun as the Earth orbits the sun. The oblateness of the Earth causes a perturbative effect that causes the RAAN to precess. This perturbation can be analyzed using the J_2 mass distribution model. Trajectory designers can choose a specific inclination for a given altitude where the perturbation causes the orbit to precess ($\dot{\Omega}_{SunSync}$) at the same rate as the motion of Earth around the sun, approximately 360°/365.25 days. This keeps the relative position of the sun in relation to the orbital plane constant [8].

$$\dot{\Omega}_{SunSync}\sqrt{\frac{a^3}{\mu}} = -\frac{3R_E^2 J_2}{2a^2(1-e^2)^2}\cos(i) \tag{2.2}$$

where $\dot{\Omega}_{SunSync}$ is the angular rate of the Earth around the sun and the desired precession rate, J_2 (0.0010826) is the oblateness constant that accounts for most of the Earth's deviation from a perfect sphere [8], and R_E is the radius of the Earth (6378 km). Rearranging Eq. (2.2) and solving for inclination yields

$$i = \cos^{-1}\left(\frac{a^{\frac{7}{2}}}{\frac{2\dot{\Omega}_{SunSync}(1-e^2)^2}{3R_E^2 J_2\sqrt{\mu}}}\right) \tag{2.3}$$

Selection of semimajor axis and eccentricity yields a value for inclination that maintains orientation with the sun, which is typically around 98°. For this analysis, 6779 km was used for semimajor axis to match ISS orbit, with an eccentricity of zero. The calculated inclination was 97.03°.

Sun-synchronous orbits are unique since the orbital plane changes relative to the lunar orbital plane with a period of exactly one year. The ISS orbit precesses faster (since inclination is lower), with a period of about 72 days. GEO can be considered non-precessing, since orientation of the orbital plane remains nearly constant throughout a year (see Chapter 4). RAAN is undefined for GTO, however four departures from GTO with 90° degree offsets in argument of periapse, to analyze any variation relative to the lunar orbit. However, this variation may be caused by J_2 perturbations or initial desired orbits.

Geostationary Orbit (GEO)

GEOs have high altitude and are circular, equatorial orbits. The altitude of 35,856 km is chosen that the period of the orbit synchronizes with the rotation of the Earth [1], so the nadir of a

spacecraft in this orbit always points to the same point on the surface of the Earth. GEO is a specific case of geosynchronous orbit with zero inclination.

Geosynchronous Transfer Orbit (GTO)

GTOs have high eccentricity and, as the name illustrates, are used to transfer to geosynchronous orbits or as a parking orbit for deep space missions [9]. This thesis uses GTO with no inclination and with perigee at 6779 km (to match the two LEOs) and apogee at an altitude corresponding to GEO for analysis.

Hohmann Transfer

A Hohmann transfer [10] is the minimum-ΔV two-burn, coplanar transfer orbit of a two body system using impulsive thrust, with optimality proven in multiple ways [11][12][13][14][15][16][17]. The Hohmann transfer applies the impulsive burns at periapse (the highest speed point on the transfer ellipse) on the lower, faster orbit, and at apoapse (the lowest speed point on the transfer ellipse) on the higher, slower orbit. Assuming a transfer from a lower circular to a higher circular orbit, the initial burn of the Hohmann transfer provides a lower bound estimate for the ΔV necessary to reach the moon, since none of the initial orbits used in this analysis are coplanar with the lunar orbit. However, the lunar gravity may provide ΔV benefits that may decrease the necessary ΔV. Figure 2.4 illustrates the Hohmann transfer.

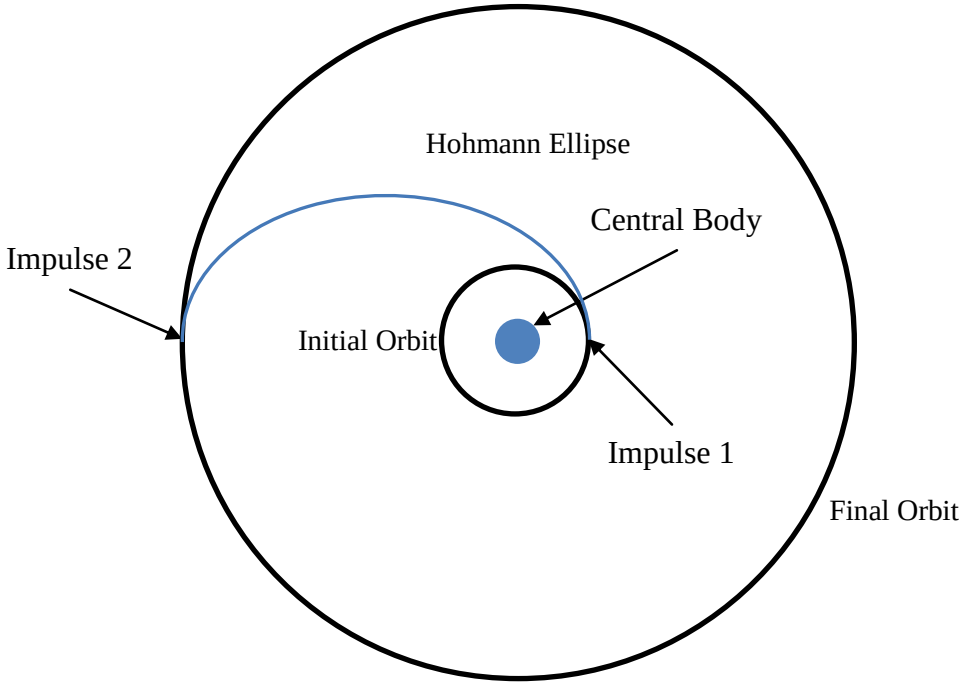

Figure 2.4: Depiction of Hohmann transfer

Lambert's Problem

Lambert's Problem consists of finding an ellipse that satisfies two given position vectors and a TOF, assuming a two-body system [18]. Finding this ellipse allows trajectory designers to find the departure and arrival velocity vectors, and consequently, the ΔV necessary to achieve this orbital transfer. Although the two-body assumption is a simplification when including the moon as part of the system, this information helps eliminate the trajectories that would require ΔV above the abilities of secondary payloads. Given a TOF and locations of the spacecraft departure and the moon, cases where the ΔV from Lambert's solution is beyond predetermined constraints can be thrown out from the onset. This drastically reduces the total computation time of the trajectory propagation.

The next chapter presents the equations and analysis techniques that utilize the parameters and tools explained in this chapter. It will lay out a framework for analyzing lunar

transfers, which can inform trajectory design and give orbit analysts better understanding of the lunar tradespace.

Chapter 3

Analysis and Equations

This analysis uses total ΔV as the performance metric order to determine the feasibility of lunar transfers. The analysis software was developed in MATLAB with the objective to simulate the ΔV tradespace. The analysis primarily covers numerically propagated trajectories for lunar flyby and crash, however there are estimates for lunar capture.

Numerical Solution

Numerical propagation, based on Cowell's method [8], was used to determine if trajectories traveled close enough to the moon. Cowell's method uses discrete function values of first-order ordinary differential equations (ODEs) to approximate solutions. When approximating position, but only have second-order equations (acceleration equations), the second-order differential equation can be rewritten as a system of first-order differential equations [6],

$$\dot{\vec{r}} = \vec{v} \tag{3.1}$$

$$\ddot{\vec{r}} = \dot{\vec{v}} = \vec{a} = -\frac{\mu}{r^3}\vec{r} \tag{3.2}$$

In this case, the numerical solver integrates a concatenated, 3D velocity and acceleration vector based on ordinary differential equations, over the specified timespan, given position and velocity initial conditions. The output is a concatenated, 3D position and velocity vector for each of the chosen time steps, which allows for easy plotting and analysis.

Cowell's method of numerical propagation was used for the ease of implementation. With this method, propagation is solved by "brute-force", where all forces acting on the body are

simultaneously integrated. Other common methods of orbit propagation are Special Perturbation methods. One such method is Encke's method. Encke's method integrates a primary acceleration along with additional accelerations linearized about multiple points along the trajectory. Special Perturbation methods can be more accurate than Cowell's method because these methods reduce the truncation error buildup. However, since this thesis focuses on the ΔV tradespace, and not the spatial accuracy, Cowell's method, along with the MATLAB differential equation solvers, provided simple, intuitive implementation with informative results. Orbital analysts may want to use a Special Perturbation method of propagation when designing trajectories that need to have increased spatial accuracy.

MATLAB ode23s

MATLAB ode23s is a numerical solver for stiff differential equations. It is based on the 2nd order Rosenbrock method [19]. The solver uses a user-defined MATLAB function that outputs the values of the ODEs. The other inputs to the solver are the timespan and initial conditions. The differential equations defined for this solver are a system of six first-order ODEs that represent the second-order, 3D gravitation system [6],

$$\ddot{\vec{r}} = \vec{a}_{Earth} + \vec{a}_{Moon} \tag{3.3}$$

where $\vec{r}$ is a spatial vector representing absolute position and $\vec{a}$ is the spatial acceleration vector (with subscripts corresponding to the cause), all in the ECI coordinate frame.

The typical "go-to" solver used for propagating differential equations in MATLAB is ode45. It is based on variable time-step, fourth order, Runge-Kutta numerical integration. However, this explicit solver is extremely slow to solve problems considered stiff. The implicit ode23s solver is robust to stiff problems [20] and solves them much faster, which is preferred when running the magnitude of cases as in this analysis.

Accelerations

The differential equations included the accelerations caused by the gravity of the Earth and the moon, modeled as point-masses [18]. In this model, gravity decreases with the square of distance. The direction of acceleration is in the negative direction of the relative position vector. The equations are

$$\vec{a}_{Earth} = -\frac{\mu_{Earth}}{{r_1}^3}\vec{r}_1 \tag{3.4}$$

$$\vec{a}_{Moon} = -\frac{\mu_{Moon}}{{r_2}^3}\vec{r}_2 \tag{3.5}$$

where μ_{Earth} and μ_{Moon} are the gravitational constants of the Earth and moon, respectively, and $\vec{r}_1$ and $\vec{r}_2$ signify the spacecraft position relative to the Earth and moon point-masses, respectively. These position vectors are shown in Fig. 3.1.

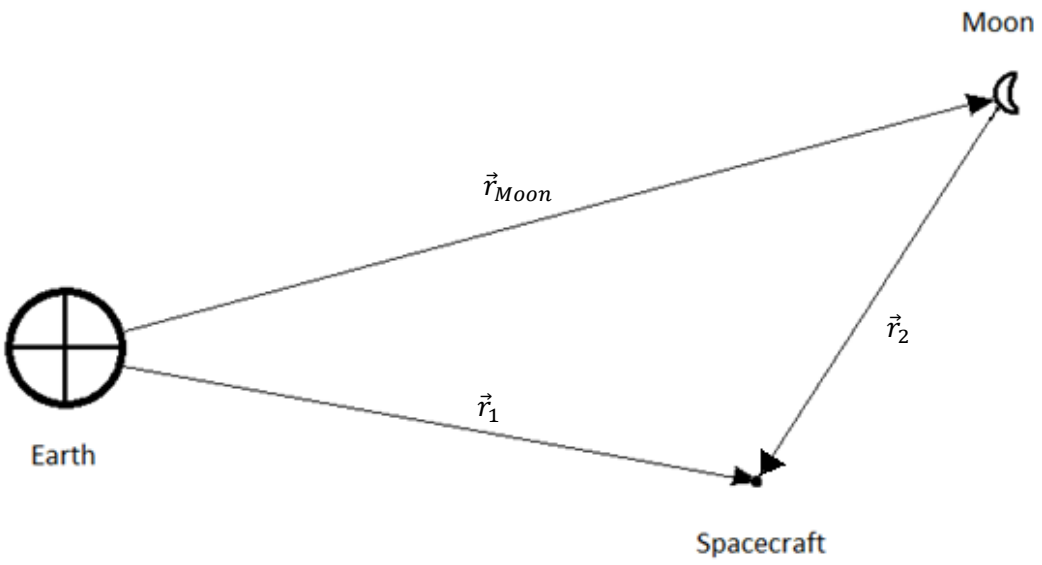

Figure 3.1: Position vector definitions

Lunar Position

To simulate the position of the moon at each time step, this analysis uses Vallado's second-order lunar ephemeris [8]. The ephemeris outputs the lunar position in the Earth-centered inertial (ECI) coordinate frame.

The position of the spacecraft relative to the moon is given by

$$\vec{r}_2 = \vec{r}_1 - \vec{r}_{Moon} \tag{3.6}$$

where $\vec{r}_{Moon}$ is the output of the Vallado ephemeris.

Stiffness

A stiff differential equation is one where the solution varies slowly in one state, but quickly in a nearby state [20]. This is case based on the proximity of the simulated spacecraft to the point-masses causing acceleration. When the spacecraft is in close proximity to the moon, the gravitational acceleration acting on the spacecraft will be orders of magnitude greater than the acceleration at the middle of the transfer trajectory. The ode23s solver is robust and speedy at solving throughout the trajectory range.

Solution to Lambert's Problem

Of the infinite possible departure vectors at a given initial position in an orbit, only a very small window of values with reasonable ΔV requirements will get the simulated spacecraft reasonably close to the moon. The solution to Lambert's problem provides a baseline translunar trajectory; a starting point for analyzing the tradespace of ΔV requirements. Lambert's problem can be described by

$$t_2 - t_1 = F(a, c, r_{depart} + r_{arrive}) \tag{3.7}$$

where t_1 and t_2 are departure and arrival times, respectively, and the difference between these times is a function of semimajor axis, chord, and arrival and departure position magnitudes, which can be seen in Fig. 3.2.

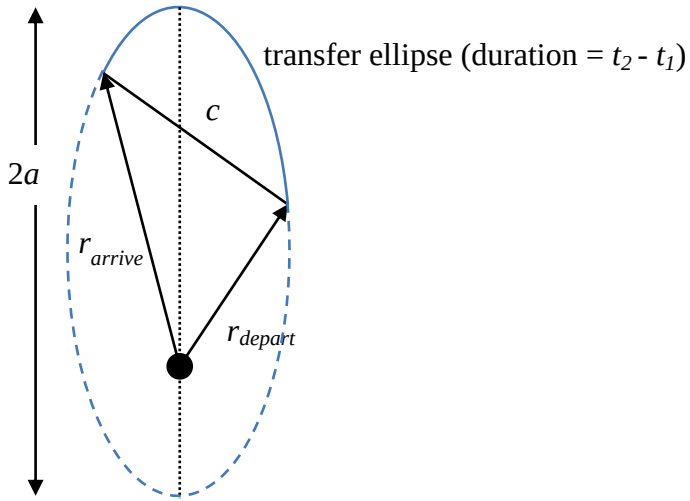

Figure 3.2: Diagram of Lambert's problem, including defining parameters

When combined with Kepler's equation, Lambert's Problem can be solved numerically by finding the value of the semimajor axis from the equation

$$\sqrt{\mu}(t_2 - t_1) = a^{\frac{3}{2}}[\alpha - \beta - (\sin\alpha - \sin\beta)] \tag{3.8}$$

with α and β (see Fig. 3.3) relations as

$$\sin\left[\frac{\alpha}{2}\right] = \left[\frac{s}{2a}\right]^{\frac{1}{2}} \tag{3.9}$$

$$\sin\left[\frac{\beta}{2}\right] = \left[\frac{s-c}{2a}\right]^{\frac{1}{2}} \tag{3.10}$$

where c is chord length between the departure and arrival position vectors, and s is the semiperimeter of the triangle defined by the two position vectors,

$$s = \frac{1}{2}\left(r_{depart} + r_{arrive} + c\right) \tag{3.11}$$

As stated by Prussing and Conway [18], the values of α and β can be interpreted as "the eccentric anomaly on the rectilinear ellipse" between the departure and arrival points (Fig. 3.3).

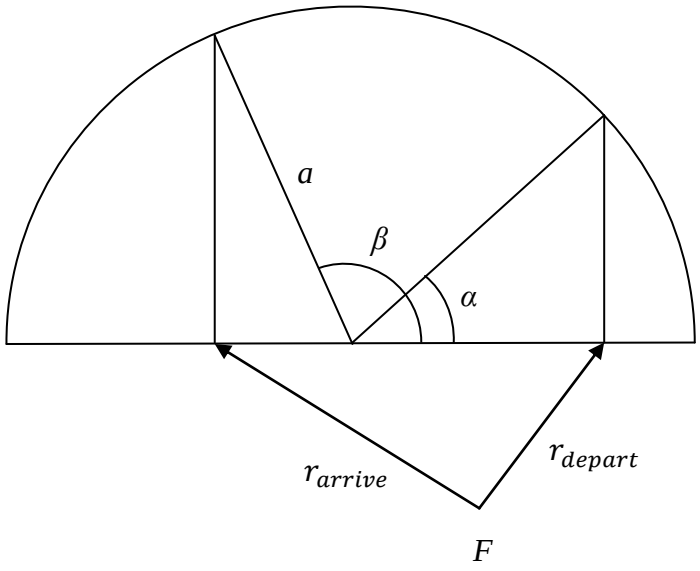

Figure 3.3: Illustration of a and b relative to departure and arrival position vectors [18]

Although the moon's gravity will have an effect, and the two-body assumption is not valid, it is a useful starting approximation for the numerical solution since the Earth's gravity has a significantly larger effect during most of the transit. The simulation used an open-source MATLAB Lambert's Problem solver developed by Oldenhuis [21], which outputted the departure velocity vector necessary for the transfer. Oldenhuis' solver finds the solution an algorithm [22] that converges quickly when few planetary revolutions are required before reaching the destination. This analysis did not require multiple revolutions, therefore this was the only algorithm that is used. Additional algorithms [23] and improvements [24] for code robustness went unused in this analysis. The output departure state vector was numerically propagated including lunar gravity and checked for minimum distance to the moon's center.

Izzo's algorithm (within the Oldenhuis solver) makes an initial guess of the minimum energy semimajor axis using non-dimensionalized position, semiperimeter, and chord. It then computes the associated time of flight using Eq. (3.8). The Newton-Raphson method is used to find the zeros of

$$y = \ln t_f - \ln t_{guess} \tag{3.12}$$

by updating t_{guess}, which is a function of the new guess for semimajor axis.

"Long Way" Solution

By default, Oldenhuis' solver solves the "short way" Lambert's solution. This is the part of the ellipse shown by the solid line in Fig. 3.2. However, the "short way" outputs massive ΔV requirements when the angle between departure and arrival position is offset by more than 180° in true anomaly. This is because the short way requires reversing the orbital direction.

The "long way" corresponds to the dotted-line section of the ellipse in Fig. 3.2. If the true anomaly offset is greater than 180°, the "long way" solution may provide the lowest ΔV transfer.

Orbital Energy

Given the two-body assumption, the energy of an orbit is given by Eq. (3.13) [18]. This energy is constant for any position throughout the orbit. This analysis uses orbital energy as a method of estimating ΔV necessary for capture.

$$constant = \varepsilon \equiv \frac{v^2}{2} - \frac{\mu}{r} \tag{3.13}$$

The algorithm for estimating capture ΔV was as follows:

1. At a state near the moon, calculate incoming orbital energy (with respect to the moon) using relative distance and speed of the spacecraft and the lunar gravitational parameter.
2. Choose a capture orbit altitude (assuming circular), which in this case was 200 km.
3. Calculate speed at capture height using incoming orbital energy.
4. Calculate orbital speed for a circular orbit at the capture height.
5. Calculate estimated ΔV by subtracting orbital speed from incoming speed at the capture height.

This equation is only valid if the impulsive, capture burn occurs at periapse of the trajectory, with respect to the moon. Trajectory designers can ensure that periapse occurs at the capture height by setting the aiming distance of the incoming trajectory [16].

Simulation Setup

The simulation consists of nested for-loops varying through initial orbit (parameters), starting date, and departure true anomaly. Figure 3.4 shows a flowchart of the simulation procedure.

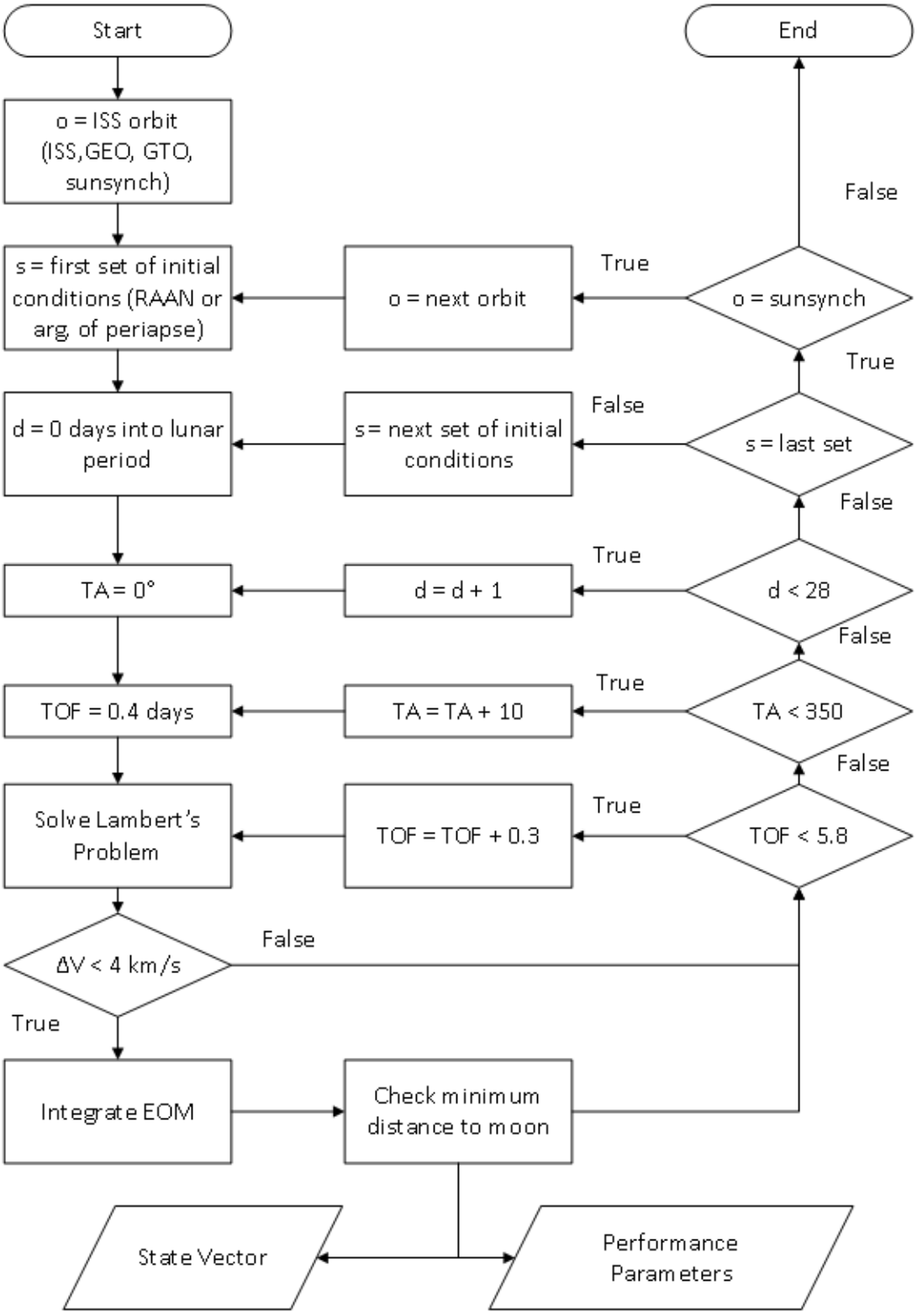

Figure 3.4: Trajectory propagation and output algorithm

1. Determine initial conditions
    a. Beginning with ISS orbit, iteratively determine initial orbit from ISS, GEO, GTO, and sun-synchronous orbit
    b. Iteratively determine the parameters of the initial orbit
        i. For ISS, RAAN takes on discrete values 0°, 90°, 180°, and 270°
        ii. For GEO, there is only one trajectory
        iii. For GTO, argument of periapse takes on discrete values 0°, 90°, 180°, and 270°
        iv. For sun-synchronous, RAAN takes on discrete values 0°, 90°, 180°, and 270°
    c. Given initial date, iteratively determine the days that have passed into the lunar period, beginning with 0 and ending at 28 (a whole period), incrementing by 1 day
    d. Iteratively determine departure true anomaly (TA), beginning with 0 and ending at 350, incrementing by 10 degrees
    e. Iteratively determine the time of flight (TOF), beginning with 0.4 days and ending at 5.8 days, incrementing by 0.3 days
2. Compute the solution to Lambert's problem given departure position (from initial orbit and true anomaly), TOF, and arrival lunar position (including TOF).
3. If case has ΔV greater than 4 km/s., check the "long way" Lambert's solution.
4. If this case ΔV greater than 4 km/s., dismiss and go back to step 1
5. Integrate using departure velocity vector.
6. Ensure that the trajectory gets close enough to the moon.
7. Output resulting trajectory (state and time vector) and performance parameters (TOF, ΔV, minimum distance to moon).

Initial Conditions

The simulation varies four parameters to achieve the Lambert's solution: initial orbit, initial orbit parameters, departure true anomaly, and TOF. These parameters were chosen so that this analysis would span the variations caused by different locations of the moon throughout the year and different approach trajectories.

Initial Orbit

There are four initial orbits used in this simulation. Common orbits are the most important to analyze for secondary payloads, since these are most likely launch opportunities. This simulation includes two low-Earth orbits (LEO, specifically the orbit of the International Space Station and sun-synchronous orbit), geotransfer orbit (GTO), and geosynchronous Earth orbit (GEO).

Initial Orbit Parameters

Variation in departure date, RAAN, and argument of periapse captures variation of the relative orientation of the initial orbits and the moon throughout a lunar period. For each initial orbit, there are 29 departure dates representing each day in the lunar period. The 1 day increment was chosen by beginning with a coarse mesh, and gradually increasing the number of increment until the shape of the minimum ΔV curve (see Chapter 4) showed continuity. This guess-and-check method helped reduce the number of cases to run while having the resolution necessary to capture variation.

Variation in RAAN allows for analysis of the variation induced by the precession caused by the J_2 perturbation, as explained in Chapter 2. Four, 90°-offset initial RAANs were used ISS

and sun-synchronous initial orbits in order to span one period of RAAN precession for the respective orbits.

For transfers from GTO, the four, 90°-offset arguments of periapse were used to define the initial orbit. These arguments of periapse are to span the set of possible GTO orientations, which may be defined by the insertion trajectory of some primary payload.

Departure True Anomaly

The simulation varies departure true anomaly every 6° throughout one period of the initial orbit, which gives 36 trajectories for each departure date. The 6° increment was chosen using the same guess-and-check method as with departure date.

Time of Flight

For each departure by true anomaly, the simulation uses a range of TOF from 0.4 days to 5.8 days. This TOF is used as an input to Lambert's problem to calculate departure velocity vector for all departures of this simulation. The minimum and maximum were chosen to bound typical lunar transfers. As with departure date and true anomaly, a 0.3 day increment was chosen using the guess-and-check method previously discussed.

ΔV Bounds

In order for this simulation to have a reasonable runtime, the MATLAB script only propagates trajectories within predetermined bounds. The simulation does not include trajectories

with ΔV requirements greater than 4 km/s (from Lambert's equation). Given Tsiolkovsky's rocket equation [1]

$$\Delta V = I_{sp} g_0 \ln \frac{m_0}{m_1} \tag{3.14}$$

where I_{sp} is the rocket specific impulse, g_0 is specific gravity, and m_0 and m_1 are the initial and final masses of the spacecraft, respectively, one can solve for the ratio of initial to final mass with known ΔV and rocket I_{sp}. The difference in mass from initial to final can be assumed to be the fuel used, shown in Eq. (3.15).

$$m_0 - m_1 = m_{fuel} \tag{3.15}$$

Dividing by m_0 yields

$$1 - \frac{m_1}{m_0} = \frac{m_{fuel}}{m_0} \tag{3.16}$$

and rearranging Eq. (3.14) and substituting into Eq. (3.16) yields

$$\frac{m_{fuel}}{m_0} = 1 - e^{-\frac{\Delta V}{I_{sp} g_0}} \tag{3.17}$$

which is the equation for fuel mass percentage of the total mass. Using Eq. (3.17), the spacecraft would need to be approximately 87% fuel, assuming an I_{sp} of 200 seconds. This mass percentage is outside the capabilities of most small spacecraft [1].

The equations presented in Chapter 3 provided the foundation to analyze the described, lunar ΔV tradespace. Chapter 4 presents the results of this analysis to inform design decisions and to understand the feasibility of lunar transfer.

Chapter 4

Results and Discussion

This chapter presents the results of the simulation described in Chapter 3. The primary criteria for judging feasibility was ΔV, since this value is generic with regards to spacecraft mass and propulsion systems.

ΔV Results

The ΔV necessary for a Hohmann transfer provides a theoretical lower limit for lunar transfers (Table 4.1). When analyzing crash or flyby lunar transfers, near-Hohmann transfers occur when the moon crosses the line of nodes between the initial and lunar orbital planes. Departures that require out-of-plane motion are non-Hohmann by definition and require higher ΔV (as seen in the presented results). Any missions that require lunar capture will be non-Hohmann, since the lunar plane is offset from all the initial planes, which is true in general.

Table 4.1: Lower limit ΔV for lunar transfers from initial orbit

Initial Orbit	Hohmann ΔV (km/s)
ISS or Sun-synchronous	3.08
GEO	1.05
GTO (depart periapse)	0.68
GTO (depart apoapse)	2.48

ISS Orbit

The orbit of the International Space Station allows for spacecraft trajectories that reach the moon under the 4 km/s ΔV-budget set for this simulation. However, all possible trajectories require above 3 km/s ΔV. Figure 4.1 shows the minimum ΔV requirements by simulation departure day across four RAAN values. Given the J_2 perturbation's effect on RAAN (Eq. 2.2), it would take about 72 days for RAAN to precess 90°. Using Eq. (3.17) and the lowest calculated ΔV requirement (3.13 km/s), a spacecraft needs to have a fuel mass fraction of at least 80%, given the same 200s I_{sp}, for a flyby or crash-landing mission. Connected points on Fig. 4.1 imply continuous groupings of successful trajectories. If trajectories near these connected points meet mission requirements, trajectory analysts should look at these regimes with higher fidelity.

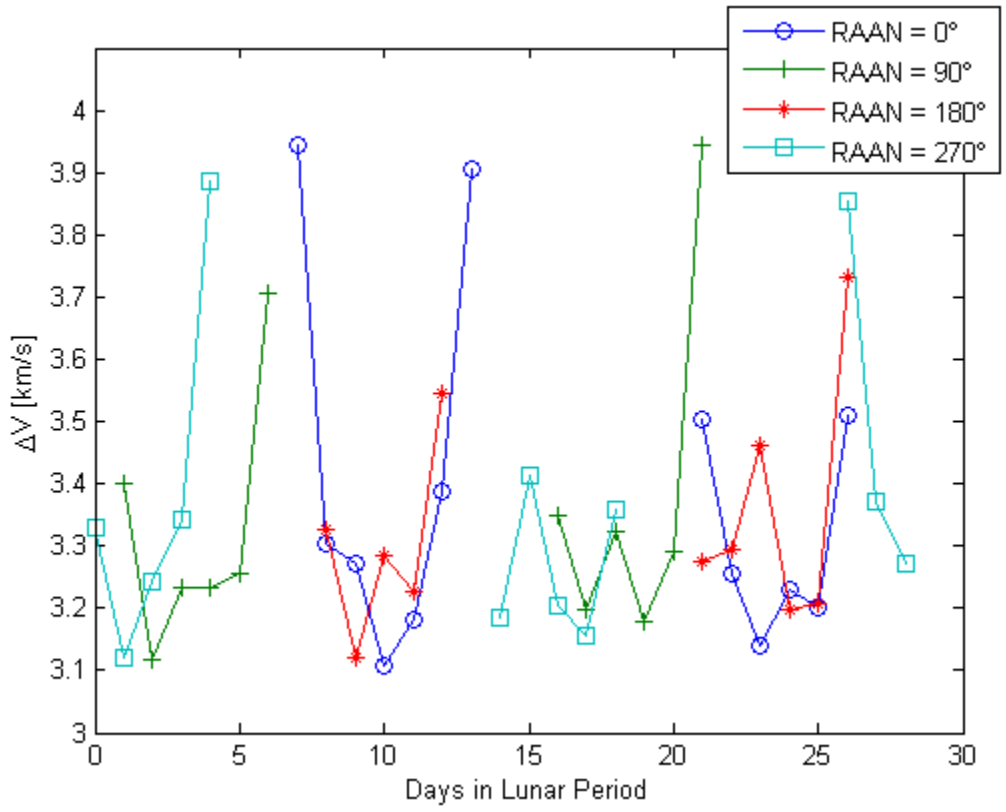

Figure 4.1: Variation of lowest simulated ΔV from ISS across the lunar period, by season.

For each initial RAAN, Fig. 4.2 shows two groupings of possible trajectories throughout the lunar period. Since the ISS orbit and the lunar orbit are non-coplanar, these two groupings correspond with Hohmann-like transfers at the ascending and descending node-lines of lunar plane with the ISS plane. The gaps in Fig. 4.2 correspond to the regions where the out-of-plane component of ΔV increase reduce the available ΔV for orbit raising to infeasibility, given the 4 km/s constraint.

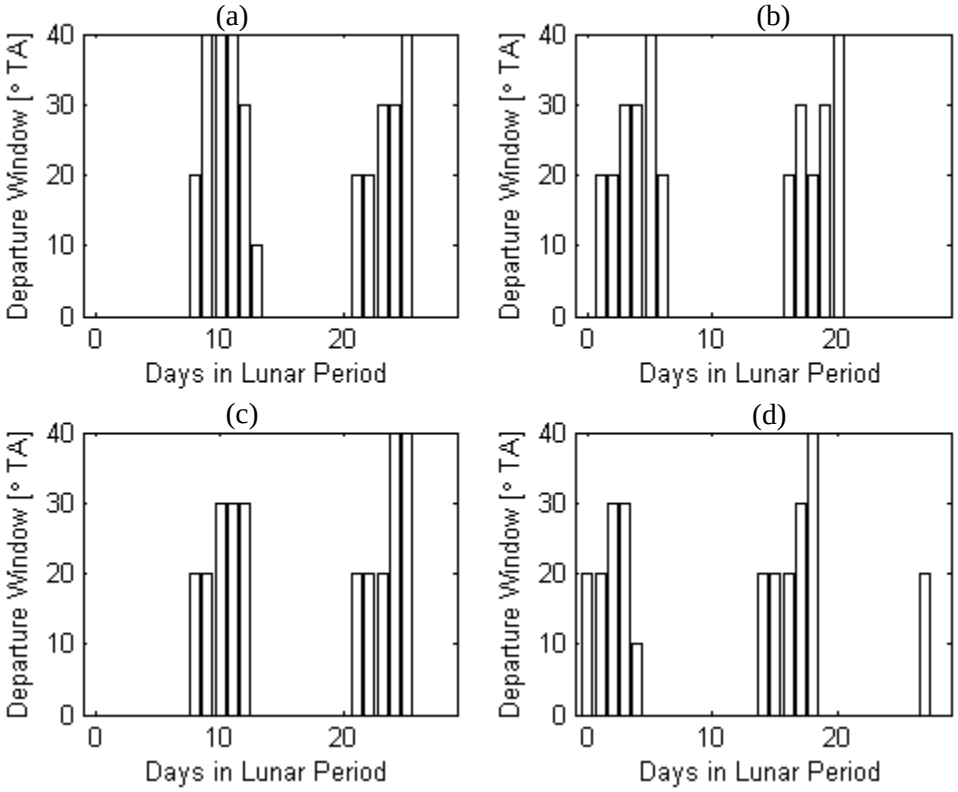

Figure 4.2: Departure windows of degrees true anomaly from ISS for every 90° of RAAN precession. (a) 0° (b) 90° (c) 180° (d) 270°

Figure 4.3 shows possible trajectories in Cartesian coordinates from the departure conditions of day 10 of a lunar period. Blue and red trajectories correspond to RAAN of 0° and 180°, respectively. Given the J_2 perturbation on RAAN, these RAANs would be separated by approximately 144 days.

Multiple clusters of trajectories can be seen, which correspond to different flight-times. Although these trajectories are clustered, the successful trajectory space is continuous. The clustering is caused by the discretization of the initial conditions. Trajectory analysts should look at the space spanned by these departure true anomalies and TOFs (Fig. 4.3) with some margin on either side to ensure all possible trajectories are included in the continuous space.

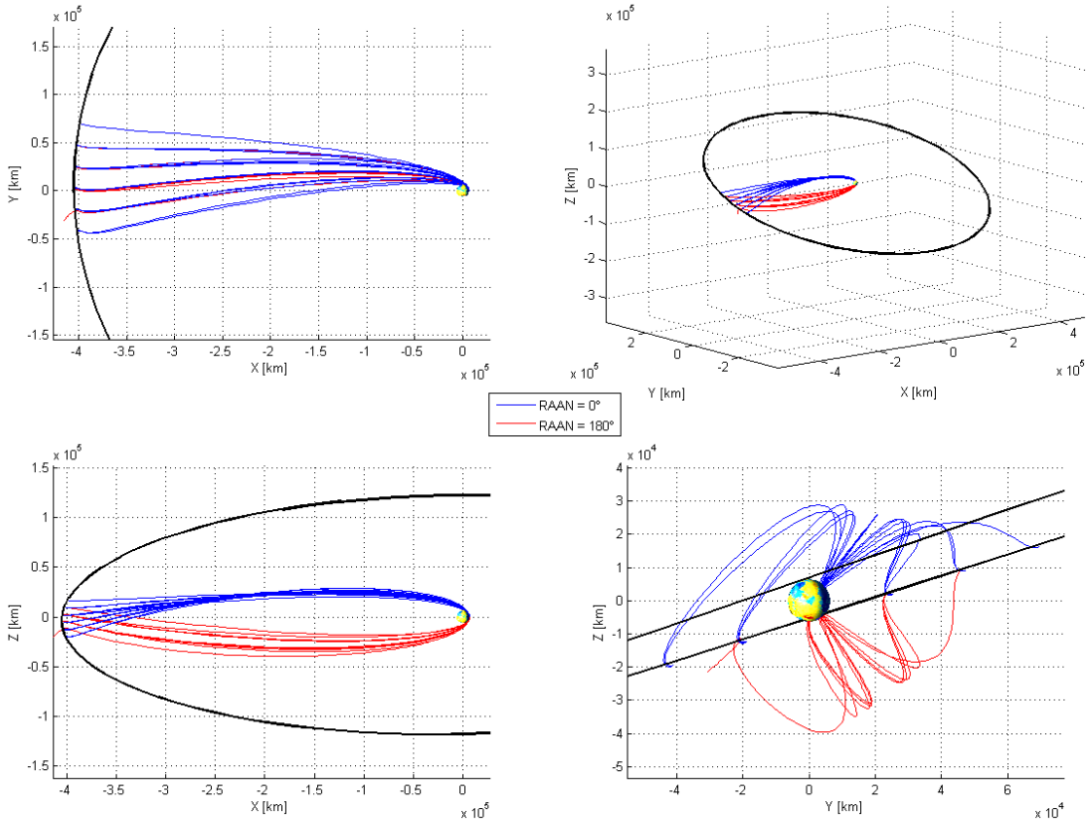

Figure 4.3: Departing ISS, 10 days into lunar period, 0° and 180° RAAN, multiple views

The departure velocity vectors lie near the orbit plane for both RAAN configurations, which is intuitive since this allows most of the impulsive energy to go toward raising the orbit to the moon, rather than changing the inclination (which does not get the spacecraft closer to the moon). If lunar capture is necessary, trajectory analysts will need to factor in the velocity of the spacecraft relative to the moon at arrival. Since the inclinations of the lunar and initial orbits do not align, out-of-plane motion will be necessary to reduce the overall ΔV costs.

As mentioned previously, the feasible trajectories occur as the moon crosses the initial orbital plane, and this can be seen in Fig. 4.3. Although RAAN is offset by 180°, the feasible trajectories occur at similar lunar locations because offset gives the same node line of initial lunar orbital planes.

GEO

A spacecraft in GEO will have no significant variation throughout the year. For equatorial orbits, RAAN is undefined because the orbit is in the same plane as the equator, thus there is no node line. For circular orbits, the argument of periapse can be defined using any point in the orbit, since there is no singular periapse. Thus, GEO will maintain orientation relative to the lunar orbit and only one orientation need be analyzed.

A spacecraft departing from GEO can reach the moon for ΔV under 2 km/s throughout the entire lunar period. This can be seen in the lack of gaps in Fig. 4.4 throughout the lunar period. Compared with the initial ISS orbit, GEO has much higher energy, and is nearly coplanar to the lunar orbit, drastically reducing the necessary ΔV. 2 km/s corresponds to approximately 64% fuel mass fraction, which is much more feasible than 90%+ for small spacecraft departing from ISS. As with the figure for ISS, connected points imply continuity.

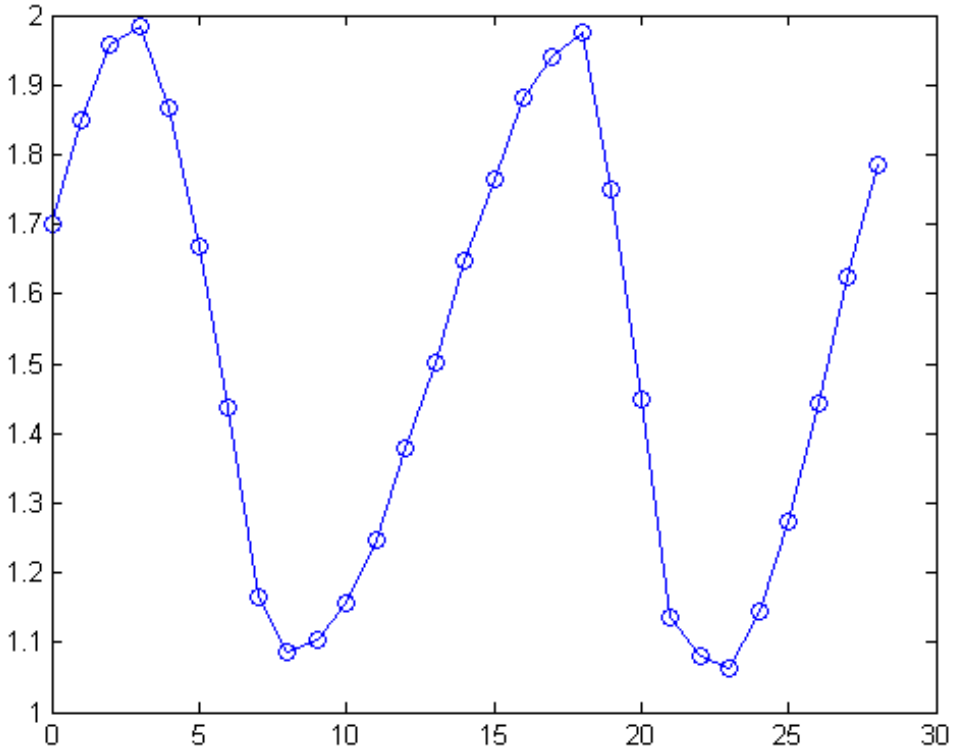

Figure 4.4: Variation of lowest simulated ΔV from GEO.

Figure 4.5 shows that a GEO departure has much larger departure windows than for ISS. The minimum window to reach the moon given the ΔV constraint is 150 degrees of true anomaly, and the maximum window is 260 degrees true anomaly. This window is much larger than for departure windows from ISS.

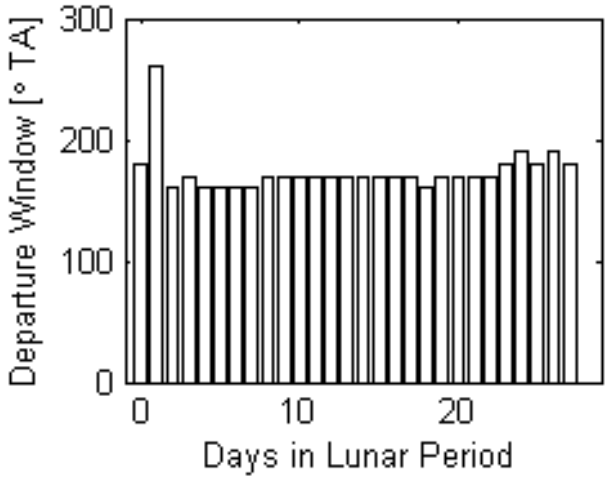

Figure 4.5: Degrees of true anomaly for departure windows from GEO

Figure 4.6 shows possible trajectories from the departure conditions of day 23 of a lunar period. This corresponds with the day into the lunar period that had the lowest calculated ΔV. As with ISS trajectories, these trajectories should be considered a continuous space, although represented discretely. The colors in Fig. 4.6 are only to help the reader differentiate between trajectories in order to imply the magnitude of possible trajectories.

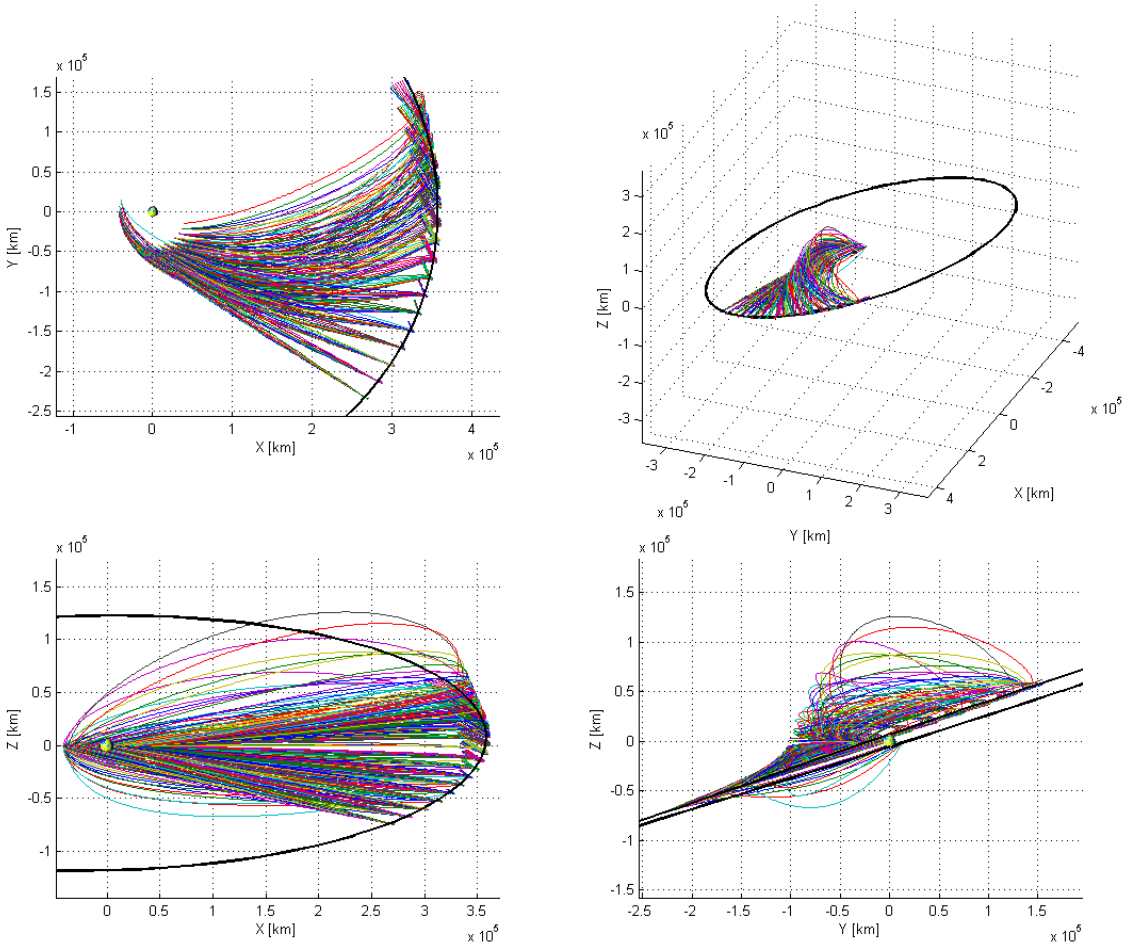

Figure 4.6: From GEO, departing 23 days into lunar period, multiple views

Trajectories diverge from the initial 0 inclination significantly, as seen in Fig. 4.6 (bottom right), which provide mission planners much more flexibility for the possibility of lunar capture (to align with lunar inclination at arrival). The increased out-of-plane motion (compared with trajectories departing from ISS) is allowed since the energy at GEO is higher. Less ΔV must be used to raise the orbit to the moon, and so some of that ΔV-energy can add to the out-of-plane motion and still be within constraints.

The feasible-trajectory-space is much larger for GEO departure than any of the other initial orbits analyzed in this thesis (Figs. 4.3, 4.6, 4.9, 4.12). A spacecraft can reach the moon from any day in the lunar period with a significant departure window. If a mission-designer

desires maximum flexibility, he or she should consider a GEO departure. However, if ΔV is a larger driver of mission success, a departure from GTO may be the best option, as seen below.

GTO

Spacecraft can reach the moon from GTO for less than 4 km/s ΔV throughout most of the lunar period. However, the most fuel efficient departures happen near the GTO periapse, since that location has a high speed (along with GTO being much higher energy than LEO), with possible transfers costing less than 1 km/s. This corresponds to necessary fuel mass fractions of less than 40%.

The curves in Fig. 4.7 corresponding to 0° and 90° argument of periapse dip down lower since these orientations align the periapse opposite the node-line of the lunar plane and the initial orbital (and equatorial) plane. As for the trajectories with GEO and ISS initial orbits, the lowest cost trajectories occur near the node line of the initial and lunar orbital planes. However, with GTO departure, there is a ΔV bonus caused by the high speed at periapse. The higher ΔVs corresponding to arguments of periapse of 90° and 270° are due to the offset of the lunar node-line and the vector pointing to periapsis.

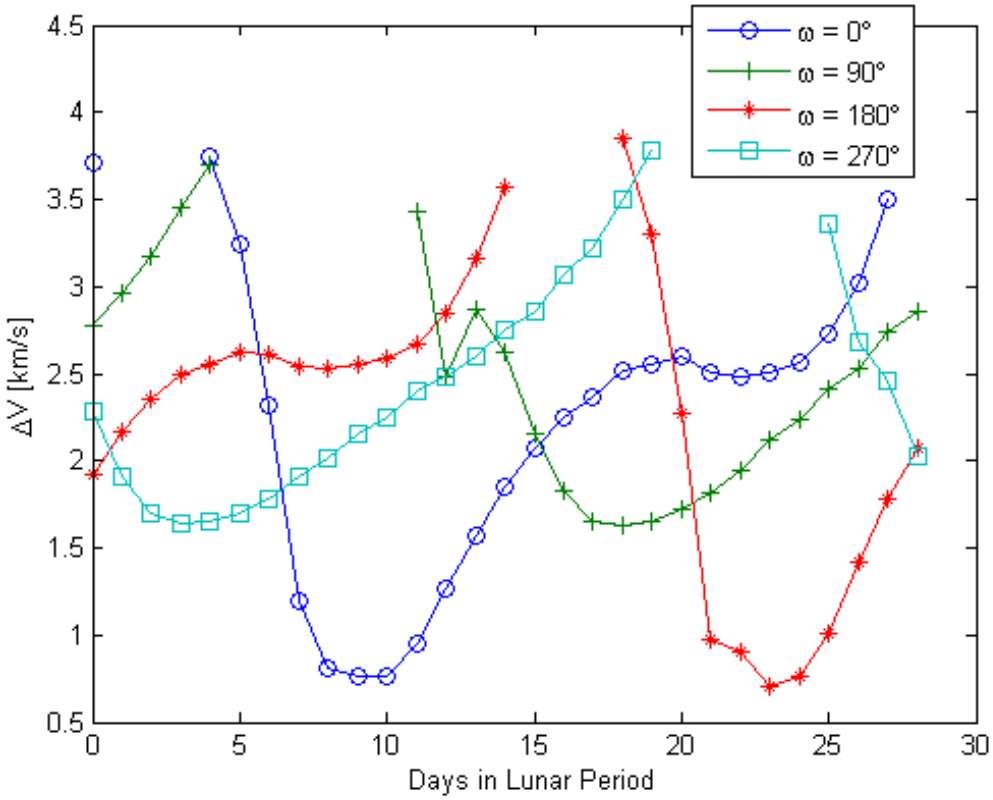

Figure 4.7: Variation of lowest simulated ΔV from GTO across the lunar period, varying argument of periapse.

Departures windows vary greatly throughout the lunar period, but are on the same order as GEO departure windows for some days throughout the lunar month. This can be seen in Fig. 4.8. GTO departures may provide trajectory designers a balance of window size and ΔV costs.

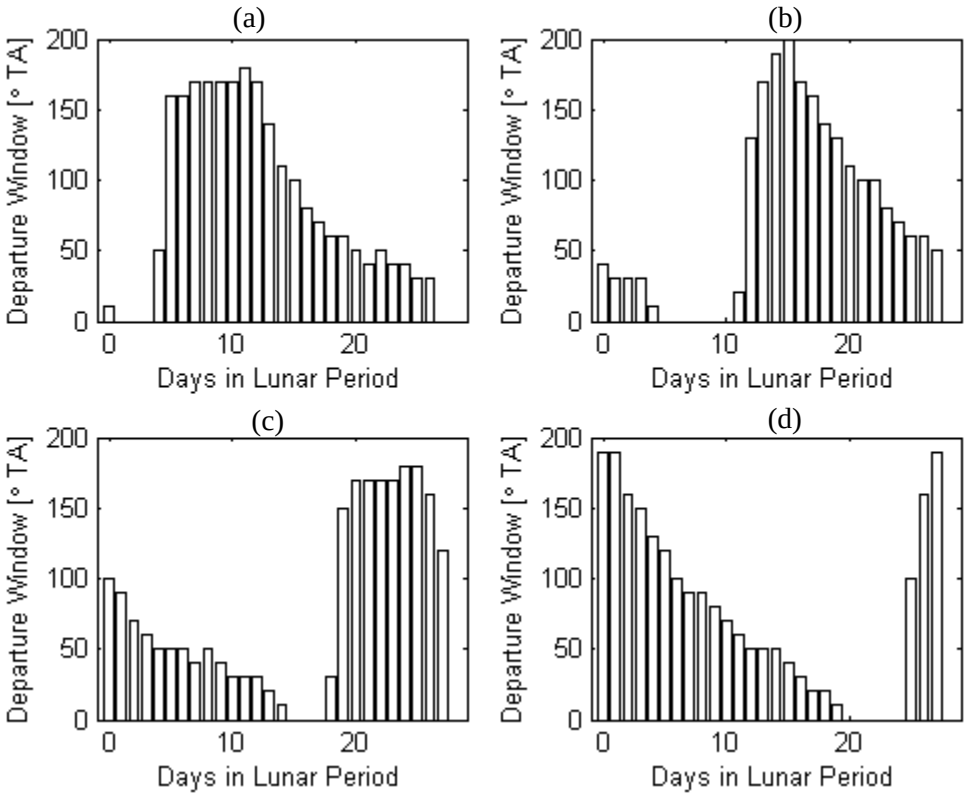

Figure 4.8: Departure windows of degrees true anomaly from GTO for every 90° of argument of periapse. (a) 0° (b) 90° (c) 180° (d) 270°

Figure 4.9 shows possible trajectories from the GTO departure with an argument of periapse of 180° corresponding to the orientation the gives the lowest ΔV. As with ISS and GEO trajectories, these trajectories should be considered a continuous space, although represented discretely. The feasibility-space is large; much larger than for ISS departure, although smaller than for GEO departures.

As seen in Fig. 4.9 (bottom right), transfer trajectories have inclinations near the initial 0 inclination (just enough out-of-plane velocity to hit the moon). As with previous trajectories, this allows the impulsive energy to be used to raise the orbit, rather than for the out-of-plane motion.

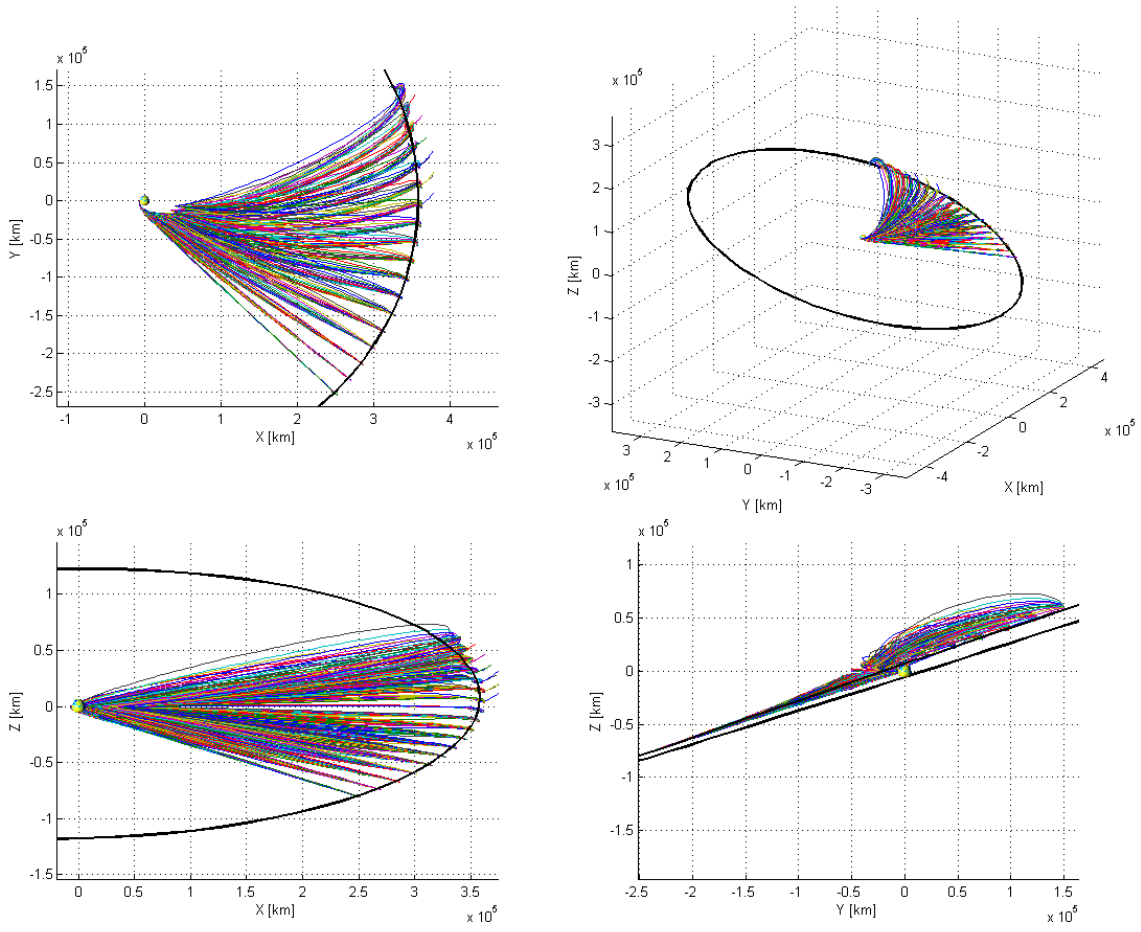

Figure 4.9: Departing GTO, departing 23 days into lunar period, argument of periapse is 180°, multiple views

Sun-synchronous

As with departures from ISS, departures from sun-synchronous orbit require much higher ΔV due to the low orbital energy. This leads to the large gaps in Fig. 4.10, where the minimum ΔV is above the 4 km/s limit. The points that show up come in two clusters, which correspond to days in the lunar period where the moon is crossing the initial orbital plane.

Acceptable trajectory departure and arrival points align with the node-lines, as with LEO trajectories. The spacecraft velocity vector at arrival is also nearly perpendicular to the lunar

velocity vector, making capture from polar orbit much more ΔV-expensive than LEO (see Table 4.2).

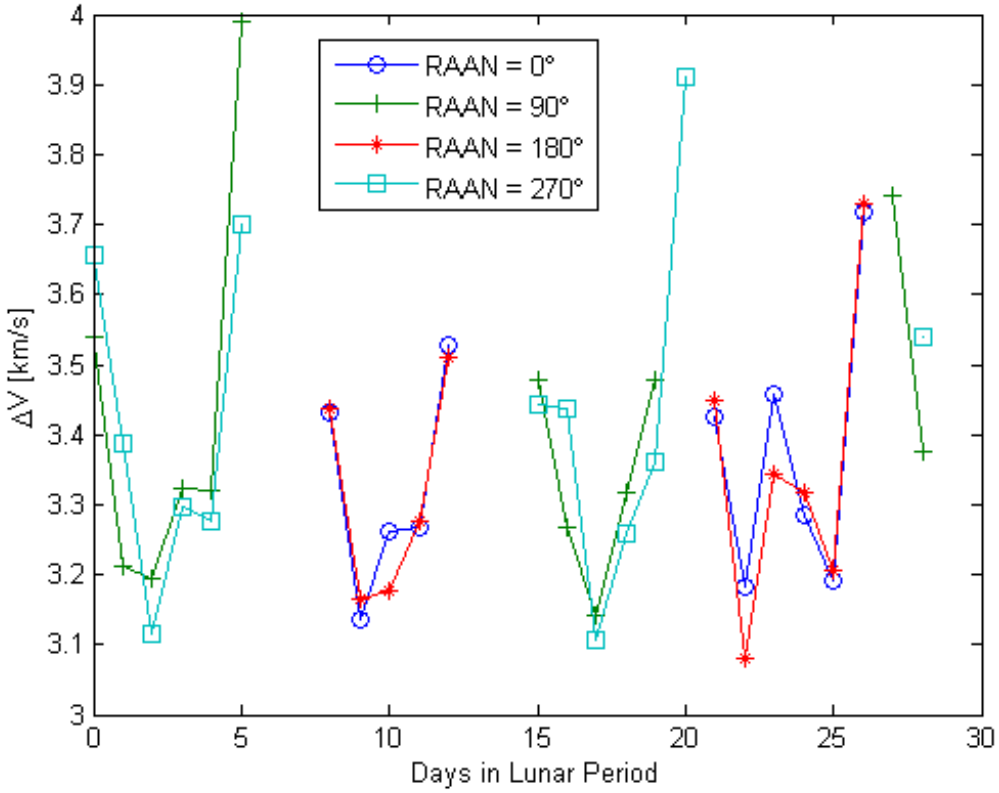

Figure 4.10: Variation of lowest simulated ΔV from sun-synchronous across the lunar period, by RAAN offsets.

One would expect performance of trajectories from sun-synchronous orbit to be nearly identical to those of ISS departures, excluding capture, and this is the case. The lowest ΔV throughout the lunar period from sun-synchronous orbit have the same approximate range as for ISS departures (Fig. 4.1). Departure true anomaly windows for sun-synchronous departure (Fig. 4.11) are on the same order as the windows for departing from ISS.

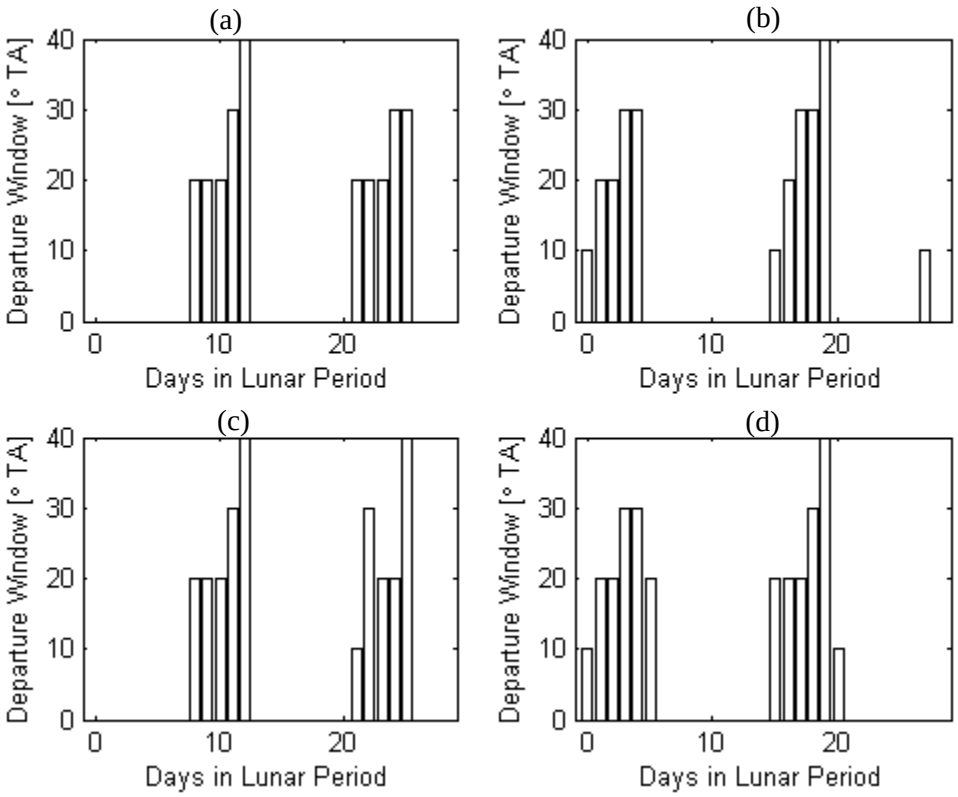

Figure 4.11: Departure windows of degrees true anomaly from sun-synchronous for every 90° of RAAN precession. (a) 0° (b) 90° (c) 180° (d) 270°

Trajectories from sun-synchronous orbit look nearly identical to those from ISS. Figure 4.12 shows possible trajectories from sun-synchronous orbit for RAAN of 0° and 180° (about 183 days apart give J_2 RAAN perturbation). As with ISS, GEO, and GTO trajectories, these trajectories should be considered a continuous space, although represented discretely. The major difference in sun-synchronous from ISS trajectories is that the departure angle is nearly perpendicular to the equatorial plane, as would be expected for initial orbits with inclinations near 90°.

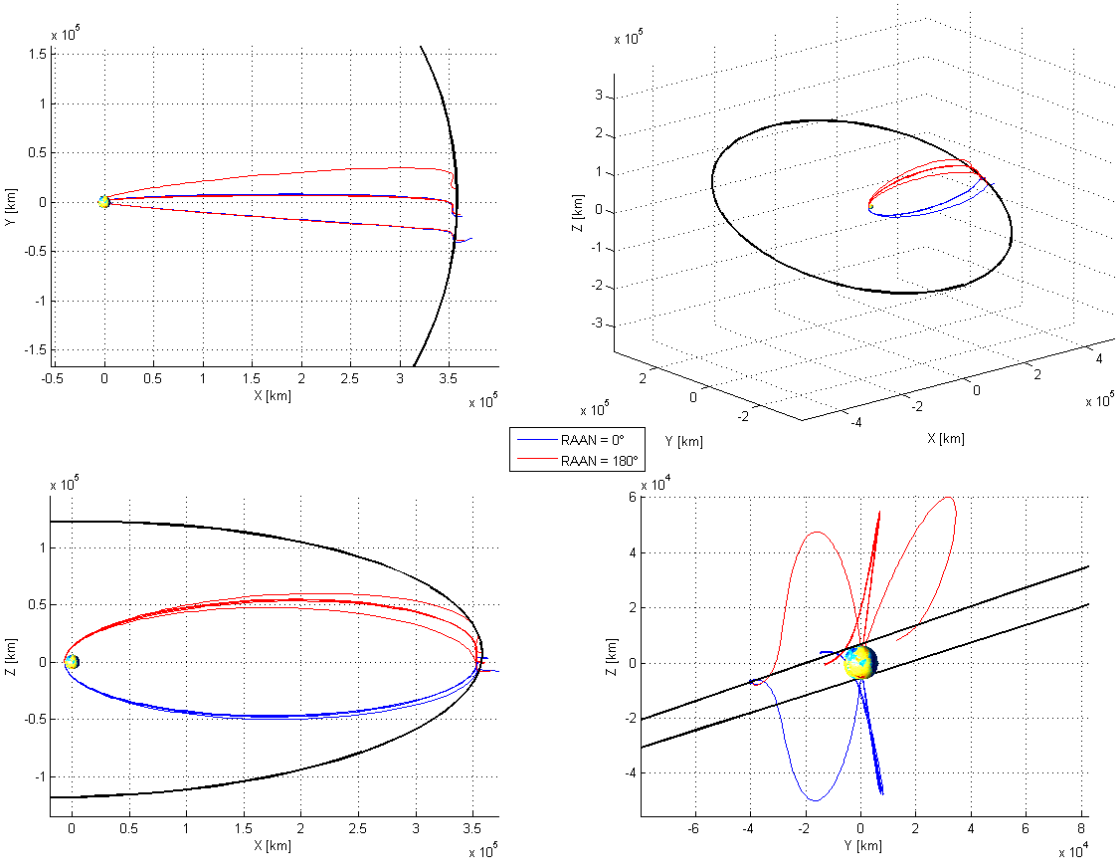

Figure 4.12: Departing sun-synchronous, 22 days into lunar period, 0° and 180° RAAN, multiple views

As with departure from ISS, acceptable trajectories from sun-synchronous travel near the departure orbital plane, where ΔV costs are minimal. As RAAN precesses 90° each season (caused by oblateness perturbation), so does the viable trajectory-space. Because of the circularity of both orbits, the ΔV remain very similar (and near Hohmann) throughout the RAAN variation, with the ΔV variation being accounted by changes in departure true anomaly.

Capture

Although this analysis focused mainly on reaching the moon, Table 4.2 presents the estimated capture ΔV for quick reference (see Appendix A for sample calculation). The capture estimate uses the trajectories from each initial orbit with the lowest departure ΔV. The total ΔV estimates are non-optimal, because minimum departure ΔV does not correspond with minimum capture ΔV, in general. The total capture optimal ΔV may require some combination of non-optimal departure and capture burns. However, that analysis is beyond the scope of this thesis.

Table 4.2: Capture ΔV for best departure trajectories.

Initial Orbit	Lowest Calculated Departure ΔV (km/s)	Estimated Capture ΔV (km/s)	Required Fuel Mass (%)
ISS	3.1	1.6	91
GEO	1.1	0.9	64
GTO	0.7	1.3	64
Sun-synchronous	3.1	3.7	97

Chapter 5

Conclusions

GEO and GTO are the ideal starting orbits for lunar missions because they have the lowest transfer ΔV's, lowest capture ΔV's and largest departure windows with respect to true anomaly. If the system has tighter ΔV contraints, spacecraft should depart from GTO, since that initial orbit allows for the lowest total to reach the moon. However, departures from GEO allow for much more flexibility in terms of departure window with minimal ΔV costs. Flyby or crash missions are feasible from ISS and sun-synchronous orbit, but capture is likely infeasible, especially from sun-synchronous, given existing propulsion capabilities.

In regards to capture departing from ISS, the 91% capture fuel mass fraction of required may be overly ambitious given the state of today's propulsion technology. The required capture ΔVs for GEO and GTO ended up the same. The capture burn for GEO was less, at 0.9 km/s, because the transfer from GEO has less relative velocity to the moon. Capture ΔV from sun-synchronous is much worse because the arrival is nearly perpendicular to the lunar plane. This requires reducing the perpendicular velocity and adding the parallel velocity, which at 97% fuel mass fraction, is a high cost. Without an improvement in technology, lunar capture from sun-synchronous should be avoided.

Future work

For lunar missions involving small spacecraft, future work should analyze two main areas: finite burn propulsion and optimal capture, descent, and landing. Analysis for finite burn propulsion removes the impulsive-ΔV assumption. This increases the complexity for determining

the optimal burns, and adds in the effects of gravity loss. The optimal capture, descent, and landing problem can be broken up in many ways, where improved overall ΔV minimization requires increased problem complexity.

References

[1] Wertz, J. R., Everett, D. F., Puschell, J. J., *Space Mission Engineering: The New SMAD*, 1st ed., Microcosm, California, 2011, Chaps. 9, 10, 18.

[2] "Capabilities and Services," Space Exploration Technologies [online], http://www.spacex.com/about/capabilities, [retrieved 26 October 2015].

[3] "Cubesat Specification," California Polytechnic State University Cubesat drawing [online], February 2014, http://www.cubesat.org/images/developers/spec_dwgs_rev13cds.pdf, [retrieved 11 October 2015].

[4] "CubeSat Modular Propulsion Systems," Aerojet Rocketdyne [online], http://www.rocket.com/cubesat, [retrieved 8 November 2015].

[5] "Secondary Payload Planner's Guide For Use On The EELV Secondary Payload Adapter", Version 1.0, DoD Space Test Program, 2001, http://everyspec.com/USAF/USAF-General/download.php?spec=DOD_STP_ESPA_Payload_Planners_Guide.005582.pdf, [retrieved 30 November 2015].

[6] Curtis, H. D., *Orbital Mechanics for Engineering Students*, 2nd ed., Elsevier, Oxford, 2010, Chap 4, 8.

[7] "Reference Guide to the International Space Station," National Aeronautics and Space Administration [online], http://www.nasa.gov/sites/default/files/atoms/files/np-2015-05-022-jsc_iss_utilization_guide_2015-508c.pdf, [retrieved 25 October 2015], pp. 78.

[8] Vallado, D. A., *Fundamentals of Astrodynamics and Applications*, 3rd ed., Microcosm, California, Springer, New York, 2007, Chaps. 5, 8, 11.

[9] Uphoff, C., "Practical Aspects of Transfer from GTO to Lunar Orbit," Ball Space Systems Division [online NASA Archives],

http://ntrs.nasa.gov/archive/nasa/casi.ntrs.nasa.gov/19930015530.pdf, [retrieved 1 November 2015].

[10] Hohmann, W., *Die Erreichbarkeit der Himmelskorper*, Oldenbourg, Munich, 1925; also, NASA Technical Translation F-44, 1960.

[11] Lawden, D. F., *Optimal Trajectories for Space Navigation, Butterworths*, London, 1963, Chap. 6.

[12] Barrar, R. B., "An Analytic Proof that the Hohmann-Type Transfer is the True Minimum Two-Impulse Transfer," *Astronautica Acta*, Vol. 9, No. 1, 1963, pp. 1-11.

[13] Hazelrigg, G. A., Jr., "The Use of Green's Theorem to Find Globally Optimal Solutions to a Class of Impulsive Transfers," American Astronomical Society, AAS Paper 68-092, Sept. 1968.

[14] Marec, J. P., *Optimal Space Trajectories*, Elsevier, Amsterdam, 1979, Chap. 2, pp. 21-27.

[15] Battin, R. H., *An Introduction to the Mathematics and Methods of Astrodynamics*, AIAA Education Series, AIAA, New York, 1987, pp. 529-530.

[16] Palmore, J. L, "An Elementary Proof of the Optimality of Hohmann Transfers," *Journal of Guidance, Control, and Dynamics*, Vol. 7, No. 5, 1984, pp. 629-630.

[17] Prussing, J. E., "Simple Proof of the Global Optimality of the Hohmann Transfer," *Journaal of Guidance, Control, and Dynamics*, Vol. 15, No. 2, 1992, pp. 1037-1038.

[18] Prussing, J. E., Conway, B. A., *Orbital Mechanics*, 2nd ed., Oxford, New York, 2013, Chaps. 1, 5.

[19] Shampine, L. F., Reichelt M. W., "The Matlab Ode Suite," Mathworks Technical Articles [online], https://www.mathworks.com/help/pdf_doc/otherdocs/ode_suite.pdf, [retrieved 25 October 2015].

[20] Moler, C., "Stiff Differential Equations," Mathworks Technical Articles [online], 2003, http://www.mathworks.com/company/newsletters/articles/stiff-differential-equations.html?s_tid=srchtitle, [retrieved 19 October 2015].

[21] Oldenhuis, R. P. S., "Robust solver for Lambert's orbital-boundary value problem," *MATLAB Central* [online code database], http://www.mathworks.com/matlabcentral/fileexchange/26348-robust-solver-for-lambert-s-orbital-boundary-value-problem, [retrieved 2 November 2014].

[22] Izzo, D., "Global Trajectory Optimisation Problems Database," European Space Agency [online database], http://www.esa.int/gsp/ACT/inf/projects/gtop/gtop.html, [retrieved 26 October 2015].

[23] Lancaster, E. R., Blanchard, R. C., "A unified form of Lambert's theorem," *NASA Technical Note TN D-5368*, 1969.

[24] Gooding, R. H., "A procedure for the solution of Lambert's orbital boundary-value problem," *Celestial Mechanics and Dynamical Astronomy*, 48:145-165, 1990.